IEEE Access
Multidisciplinary | Rapid Review | Open Access Journal

Received June 21, 2020, accepted July 9, 2020, date of publication July 13, 2020, date of current version July 23, 2020.

Digital Object Identifier 10.1109/ACCESS.2020.3008849

BDS PPP/INS Tight Coupling Method Based on Non-Holonomic Constraint and Zero Velocity Update

WEI SUN AND YIHAN YANG
School of Geomatics, Liaoning Technical University, Fuxin 123000, China

Corresponding author: Yihan Yang (yangyihan07@163.com)

This work was supported in part by the Liaoning Revitalization Talents Program under Grant XLYC1907064, in part by the Support Plan for Innovative Talents in Colleges and Universities of Liaoning Province under Grant LR2018005, in part by the Basic Scientific Research Projects of Liaoning Higher Education Institutions under Grant LJ2017FAL005, in part by the "Liaoning BaiQianWan Talents Program" under Grant Liao BaiQianWan Program [2019] no. 45, and in part by the Beijing Key Laboratory of Urban Spatial Information Engineering under Grant 2018206.

ABSTRACT According to the problem that the positioning error increased with the increase of navigation time in the environment of complete lack of satellite signals such as viaduct and tunnel, the precise point positioning (PPP) / inertial navigation system (INS) tight coupled continuous positioning with non-holonomic constraint (NHC) and zero velocity update (ZUPT) in BeiDou navigation satellite system (BDS) was proposed. Firstly, the ionospheric composite model was analyzed from the aspects of observation equation, parameter estimation, fuzziness, degree of freedom and noise. The BDS PPP dynamic positioning model of ionospheric composite was established, and the errors that affect the positioning accuracy and convergence rate were analyzed. According to the motion characteristics of land vehicles, a scheme of velocity NHC was proposed to limit the accumulation of system positioning error with time, and ZUPT was used to increase the navigation accuracy of the integrated system when the vehicle was in the static state at the traffic light. The experimental results showed that the horizontal positioning accuracy of converged BDS PPP was better than 5 cm, the vertical positioning accuracy was better than 10 cm, and the dynamic positioning results are different from the high-precision real-time kinematic (RTK) / INS integrated navigation results by centimeters. The positioning accuracy of the system could be effectively improved by the BDS PPP/INS tight coupling method of NHC+ZUPT. Compared with the PPP/INS tight coupled positioning results without any constraints, the accuracy of the method in the three directions of East, North, and Up was increased by 0.08 m, 0.02 m and 0.01 m respectively.

INDEX TERMS BeiDou precise point positioning, velocity non-holonomic constraint, zero velocity update, tight coupled navigation.

I. INTRODUCTION

Precise point positioning (PPP) is the technique that enables centimeter- or decimeter-level positioning accuracy with only one receiver on a global scale [1], and was implemented on GIPSY software developed by themself, with positioning accuracy of 1-2cm. In 2001, Kouba and Héroux [2] of the Canadian Department of Natural Resources studied the PPP technology and realized the positioning accuracy of static data at cm level. In the next two decades, PPP technology was improved and developed continuously by the domestic and international scientific research institutions such as University of Calgary in Canada [3], German Geoscience Center GFZ [4], [5], Institute of Geodesy of Chinese Academy of Sciences [6], Wuhan University [7], and International GNSS Service (IGS) Analysis Center.

In the study of dual-frequency PPP, according to the different function models, it is mainly divided into three types: deionization combined model, University of Calgary (UofC) model and undifferenced and uncombined model. The first-order ionospheric delay was eliminated by the combined ionospheric model through the combination of

The associate editor coordinating the review of this manuscript and approving it for publication was Mu Zhou.

dual-frequency pseudorange and phase, which is one of the most widely used models at present. The UofC model was also known as semi-sum model, in which the first-order ionospheric delay was eliminated and the influence of observation noise was reduced. A new observation equation of ionospheric elimination was formed by this model through the semi-sum calculation of two-frequency pseudo distance and carrier wave. Both the deionization model and the UofC model eliminate the effect of the ionosphere through the combination of pseudorange and carrier phase observations, but the ionospheric constraints were lost, the intensity of the observation model and the fixed rate of ambiguity were reduced. In recent years, the undifferenced and uncombined model have been proposed by scholars at home and abroad, which makes full use of the observed data and the fixed rate and convergence rate of PPP fuzziness can be proved. Li *et al.* [8] analyzed the relationship between the three models, and the equivalence of the undifferenced and uncombined model and the UofC model from a fixed angle of ambiguity was proved, and they were all superior to the combined ionospheric model. In terms of ambiguity fixation, Shi and Gao [9], Ge *et al.* [10], Chen *et al.* [11] and Aggrey and Bisnath [12] carried out comprehensive analysis from the aspects of principle derivation, data verification, influencing factors and convergence time.

Chinese scholars have also made great contributions to the research of PPP technology. In 2002, Dr. Ye of Wuhan University made a more in-depth study on the undifferenced PPP technology, the undifferenced GPS data model and parameter estimation method were analyzed, the method of estimating the relative clock difference of satellite by using IGS tracking stations was proposed, and a PPP service model based on Internet was designed. The research results showed that for single-day static post-processing PPP, the convergence time was about 15 minutes. The positioning result had an accuracy of better than 2 cm in the E direction, better than 1 cm in the N direction, and better than 3 cm in the U direction [13]. Academician Liu and his team at the Satellite Navigation and Positioning Technology Research Center of Wuhan University have developed a comprehensive satellite data processing software with PPP function (Position And Navigation Data Analyst, PANDA) [14]. Geng *et al.* [15] used ultra-rapid ephemeris provided by IGS station and about 40 global reference stations to achieve real-time PPP with 10-20 cm accuracy using PANDA software. In China, only 6-7 reference stations are needed to realize real-time PPP service with 10-20cm accuracy nationwide. With the help of the ground reference station and the PANDA software of Wuhan University, Ma and Shi [16] realized the high-precision orbit determination of BeiDou satellite, whose radial accuracy was better than 10cm. Using the BDS precision ephemeris and 30 s sampling interval precision clock difference products issued by Wuhan University, a week of static and dynamic experiments was carried out on Beijing Station and Wuhan Station. The results showed that: Based on the static single-day calculation of BeiDou, the horizontal direction accuracy reached 1cm, and the up direction accuracy was 1-2 cm. After the dynamic converged, the horizontal accuracy reached 4 cm, and the up direction accuracy was 4-6 cm. After a long-term research on the theory and method of PPP technology, Professor Zhang of Wuhan University proposed the fractional bias separating (FBI) model of integer calculation of undifferenced ambiguity, and independently developed the high-PPP commercial software Trip, whose positioning results were equivalent to the international commercial software precision [17]. In addition, RTKLIB, GPSTK, PPPH and other open-source software also make PPP technology further developed and promoted [18]. At present, the main factors restricting the application of PPP technology are that the positioning accuracy in dynamic positioning is greatly affected by the environment, the convergence time is long, and the satellite needs to re-converge after interruption.

With the continuous maturity of PPP technology, PPP/INS integrated navigation has become a research hotspot in recent years. The tight coupling through airborne experiments were analyzed and the positioning accuracy was in the range of cm $\sim$ dm, and the velocity measurement accuracy was in the range of cm/s. In addition, the effect of GPS interruption time on the positioning accuracy of the loose and tight coupling was analyzed. The experiment showed that when the GPS was interrupted for 10 s, the positioning accuracy of the loose coupling drops to m level, while the tight coupling could maintain more than 30 s. Kjørsvik *et al.* [19] have proved that the tight coupling has obvious advantages over the loose coupling through vehicle experiments and airborne experiments. The tight coupling could significantly improve the positioning performance of PPP, and the accuracy was in the dm level. Du, University of Calgary, studied the tight coupling of micro electro mechanical sensors (MEMS) for low-cost inertial navigation and GPS PPP, and proposed to use INS to assist the detection and repair of GPS cycle slips. After the cycle slips are repaired, the positioning accuracy in the horizontal and up directions Increased by 21.4% and 31% respectively [20]. Liu *et al.* [21] implemented a tight coupling model of GNSS single-frequency PPP and low-cost INS, and analyzed the positioning performance when the number of satellites seen in the vehicle experiment was insufficient. The experimental results showed that the three-dimensional positioning error was within 10 m after the observation of three satellites for the next minute. Wu has realized GPS PPP/INS loose coupling in China, but the vehicle experiment results showed that the PPP accuracy did not be improved significantly by the loose coupling, and the positioning accuracy was 1.5 m [22]. Zhu deeply analyzed the PPP function model and INS error model, realized the loose coupling and tight coupling of GPS PPP/INS, and the good positioning effect was achieved in vehicle experiment [23]. Liu realized GPS PPP ambiguity fixed solution and PPP/INS tight coupling model of ambiguity fixed solution by using integer phase clock products and inter satellite single difference model. The results showed that the positioning accuracy could reach centimeter level after ambiguity fixed, the velocity and attitude accuracy were

equivalent to DGNSS/INS combination accuracy, and INS could speed up the re-fixed time of PPP under the condition of poor signal [24]. Han improved the PPP/INS tight coupling algorithm by using the prior information constraint of tropospheric delay, and the positioning accuracy was improved to a certain extent [25]. Li analyzed the positioning, velocity measurement and attitude performance of the tight coupling. The results of vehicle experiments showed that the positioning accuracy was dm level, the velocity accuracy was better than dm/s level, and the attitude angle error was within 1° [26]. Gao conducted a full analysis of the loose and tight coupling. The vehicle experimental results showed that the positioning accuracy of the loose coupling was dm level, the velocity accuracy was cm/s level, and the attitude angle error was better than 0.15°. The result of tight coupling navigation was significantly improved compared with that of loose coupling. The positioning accuracy was cm level, the velocity accuracy was cm/s level, and the attitude angle error was better than 0.1° [27]. In addition, the comparative study on the loose coupling and tight coupling of BDS+GPS PPP/INS was also carried out. The experimental results showed that the tight coupled positioning accuracy was better than the loose coupling and the convergence rate of PPP under the constraints of INS could be accelerated [28].

Aiming at the problem of large error (position discontinuity) in PPP/INS positioning results in complex environment, and the increasing positioning error with the increase of navigation time in the environment of complete lack of satellite signals, such as viaduct and tunnel, the tight coupling of BDS PPP positioning and BDS PPP/INS with velocity NHC were proposed. According to the characteristics of land vehicles, velocity NHC were used to limit the accumulation of errors, and the ZUPT principle is used to increase the navigation accuracy of the integrated system when the vehicle is at the traffic lights, and the effectiveness of the proposed method was verified through experiments.

The structure of the paper is as follows. In Section II, the ionospheric dissipation combined model is established as the function model of BDS PPP, and the quality of the original data is analyzed from the data integrity rate, MP1, MP2, cycle slip ratio and code minus carrier. In Section III, velocity NHC and ZUPT principle are proposed, and then on this basis, the NHC+ZUPT BDS PPP/INS tight coupling continuous positioning solution and the specific algorithm implementation process is proposed. Experiment results with the proposed method are shown and discussed in Section IV. Finally, the conclusion is drawn in Section V.

II. BDS PPP MODELING AND ACCURACY ANALYSIS

PPP technology uses the pseudorange and phase observations of a single receiver in combination with the precise products provided by the international GNSS service organization (IGS) to obtain the positioning results at centimeter level. PPP technology has been widely used in marine surveying and mapping, seismic monitoring, aerial photogrammetry and other fields because of its advantages of high positioning accuracy, no need of reference station and low operation cost. The main content of this section is to establish the combined model of ionospheric dissipation and to explain and analyze the data quality indicators that affect the accuracy of PPP.

A. COMBINED MODELING OF IONOSPHERIC DISSIPATION OF BDS

The essence of satellite positioning is to calculate the position of the receiver by the rear intersection, which is based on the position of the satellite and the propagation distance from the receiver to the satellite. The PPP technology is to calculate the precise position of the receiver according to the precise position of the satellite (xxxx.sp3), the precise clock difference of the satellite (xxxx.clk) and various appropriate error processing strategies.

For pseudorange and phase observations of a satellite at any frequency, the following observation equations can be obtained:

$$\begin{cases} P_i = \rho + cdt_r - cdt^s + dtrop + dion_i + b^r_{P_i} + b^s_{P_i} + \varepsilon_{P_i} \\ L_i = \rho + cdt_r - cdt^s + dtrop - dion_i + b^r_{L_i} + b^s_{L_i} - \lambda_i N_i + \varepsilon_{L_i} \end{cases} \tag{1}$$

where the subscript r and superscript s represent receiver and satellite respectively. Subscript i represents carrier frequency, taking 1 and 2 P_i represents pseudorange original observation value in meters. L_i represents carrier phase original observation value in meters. ρ represents geometric distance between receiver and satellite in meters. c represents light velocity (m/s) in vacuum. dt_r and dt^s represents receiver clock difference and satellite clock difference in seconds respectively. $dtrop$ represents tropospheric delay in meters. $dion_i$ represents the ionospheric delay in meters at i frequency. λ_i represents the corresponding wavelength in meters. N_i represents integer ambiguity in cycles. λ_i and $b^r_{L_i}$ represents receiver pseudorange and phase deviation respectively in meters. $b^s_{p_i}$ and $b^s_{L_i}$ respectively represent the pseudorange and phase deviation of satellite end in meters. ε represents the corresponding observed noise in meters including the multipath error.

According to the characteristic that ionospheric delay is inversely proportional to the square of signal frequency f, two frequencies are used to form a combined ionospheric model. The pseudorange and phase observation equations of dual frequency GNSS receiver can be expressed as follows:

$$\begin{cases} P_1 = \rho + cdt_r - cdt^s + dtrop + dion_1 + b^r_{P_1} + b^s_{P_1} + \varepsilon_{P_1} \\ P_2 = \rho + cdt_r - cdt^s + dtrop + dion_2 + b^r_{P_2} + b^s_{P_2} + \varepsilon_{P_2} \\ L_1 = \rho + cdt_r - cdt^s + dtrop - dion_1 + b^r_{L_1} + b^s_{L_1} \\ \qquad - \lambda_1 N_1 + \varepsilon_{L_1} \\ L_2 = \rho + cdt_r - cdt^s + dtrop - dion_2 + b^r_{L_2} + b^s_{L_2} \\ \qquad - \lambda_2 N_2 + \varepsilon_{L_2} \end{cases} \tag{2}$$

For the combination of pseudorange P_1, P_2, phase L_1, L_2 with the ionospheric desorption, the following can be

obtained:

$$\begin{cases} P_{IF} = \alpha P_1 + \beta P_2 = \rho + \left(cdt_r + b^r_{P_{IF}}\right) - \left(cdt^s - b^s_{P_{IF}}\right) \\ \qquad + dtrop + \varepsilon_{P_{IF}} \\ L_{IF} = \alpha L_1 + \beta L_2 = \rho + \left(cdt_r + b^r_{L_{IF}}\right) - \left(cdt^s - b^s_{L_{IF}}\right) \\ \qquad + dtrop - \lambda_{IF} N_{IF} + \varepsilon_{L_{IF}} \end{cases} \tag{3}$$

$$cdt^r_{P_{IF}} = cdt_r + b^r_{P_{IF}} \tag{4}$$

$$cdt^s_{P_{IF}} = cdt^s - b^s_{P_{IF}} \tag{5}$$

$$cdt^r_{L_{IF}} = cdt_r + b^r_{L_{IF}} \tag{6}$$

$$cdt^s_{L_{IF}} = cdt^s - b^s_{L_{IF}} \tag{7}$$

where $\alpha = f_1^2/\left(f_1^2 - f_2^2\right)$, $\beta = -f_2^2/\left(f_1^2 - f_2^2\right)$ represents the ionospheric combination coefficient. For the BeiDou ii satellite, the frequency of B1 is $f_1 = 152.6 \cdot f_0$, and the frequency of B2 is $f_1 = 118 \cdot f_0$, where $f_0 = 10.23MHz$, and $\alpha \approx 2.487$, $\beta \approx 1.487$. P_{IF} and L_{IF} represent the combined values of pseudorange and phase deionization layer respectively. λ_{IF} and N_{IF} represent the combined wavelength and ambiguity of deionization layer respectively. Equations (4) $\sim$ (7) are the four types of clock errors defined. The idea is to estimate or correct the corresponding deviation term together with the actual clock error dt_r of the receiver and the actual clock error dt^s of the satellite. By using the satellite clock differential products $dt^s_{P_{IF}}$ provided by IGS, equations (4) and (5) are substituted into equation (3) to obtain:

$$\begin{cases} P_{IF} = \rho + cdt^r_{P_{IF}} - cdt^s_{P_{IF}} + dtrop + \varepsilon_{P_{IF}} \\ L_{IF} = \rho + cdt^r_{P_{IF}} - cdt^s_{P_{IF}} + dtrop - \lambda_{IF} N_{IF} \\ \qquad + \left(b^r_{L_{IF}} + b^s_{L_{IF}}\right) - \left(b^r_{P_{IF}} + b^s_{P_{IF}}\right) + \varepsilon_{L_{IF}} \end{cases} \tag{8}$$

As it shown that, for the users, when the clock difference $dt^s_{P_{IF}}$ which provided by IGS is used for PPP, assuming that n satellite in one epoch are observed, $2n$ observation equation of the epoch are obtained, and the parameters to be estimated are: 3 position coordinates of the carrier, 1 clock error of the receiver $dt^r_{P_{IF}}$ including the pseudorange error of the receiver client, 1 delay of the troposphere, $n - \lambda_{IF} N_{IF} + \left(b^r_{L_{IF}} + b^s_{L_{IF}}\right) - \left(b^r_{P_{IF}} + b^s_{P_{IF}}\right)$(estimated as a whole). There are $3 + 1 + 1 + n = 5 + n$ parameters in total, and the degree of freedom is $2n - (5 + n) = n - 5$. It indicates that at least 5 satellites need to be observed to perform precise single-point positioning calculation [29]. Because the ambiguity is affected by $\left(b^r_{L_{IF}} + b^s_{L_{IF}}\right) - \left(b^r_{P_{IF}} + b^s_{P_{IF}}\right)$, if the user fix the ambiguity by using the combined ionospheric model, it is necessary to correct or eliminate the four types of clock differences, and decompose the ambiguity into wide and narrow lanes to solve step by step.

Pseudorange observation noise is much larger than carrier phase observation noise, assuming that $\varepsilon_{P_1} \approx \varepsilon_{P_2}$, there are:

$$\varepsilon_{P_{IF}} = \sqrt{\left(\alpha\varepsilon_{P_1}\right)^2 + \left(\alpha\varepsilon_{P_2}\right)^2} \approx 3\varepsilon_{P_1} \tag{9}$$

The ionospheric noise is about three times of the original observed noise.

B. BDS DATA QUALITY ANALYSIS

The quality of the positioning results is influenced by the GNSS data quality. The performance of a receiver and the surrounding environment are reflected by the quality of the original observation data of the receiver. At present, the main test indicators of data quality include data integrity rate, first-frequency multipath effect (MP1), second-frequency multipath effect (MP2), cycle slip ratio and code minus carrier. The specific calculation formula and definition are as follows:

1) DATA INTEGRITY RATE

During data collection, the percentage of the actual observation epoch and the theoretical observation epoch of the receiver is the data integrity rate, and the calculation formula is as follows:

$$\alpha = \frac{N_i}{N_0} \times 100\% \tag{10}$$

where α represent data integrity rate, N_i represent the actual observation epoch, and N_0 represent the theoretical observation epoch. The completeness of the observed data is reflected by the data integrity rate. The ideal data integrity rate is equal to 100%.

2) MP1

MP1 is the influence index of multipath effect on pseudorange and phase at the first frequency of the observed signal. The larger the value of MP1, the greater the influence of the multipath effect produced by the observation environment. The calculation formula of MP1 is as follows:

$$MP_1 = P_1 - \left(1 + \frac{2}{\alpha - 1}\right)\varphi_1 + \frac{2}{\alpha - 1}\varphi_2 \tag{11}$$

where P_1 represents pseudorange observations on the first frequency, φ_1 and φ_2 represent phase observations on the first and second frequencies respectively, $\alpha = (f_1/f_2)^2$, f_1 is the first frequency, f_2 is the second frequency.

3) MP2

MP2 is the influence index of multipath effect on pseudorange and phase at the second frequency of the observed signal. The larger the value of MP2, the greater the influence of the multipath effect produced by the observation environment. The calculation formula of MP2 is as follows:

$$MP_2 = P_2 - \frac{2\alpha}{\alpha - 1}\varphi_1 + \left(\frac{2\alpha}{\alpha - 1} - 1\right)\varphi_2 \tag{12}$$

where P_2 represents pseudorange observations on the second frequency.

4) CYCLE SLIP RATIO

Cycle slip is a jump in the value of the receiver's full-cycle counter due to the loss lock of the satellite signals. The indicator reflecting the cycle slip is defined as:

$$o/slps = \frac{num\_of\_obs}{num\_of\_slips} \tag{13}$$

where o/slps represents the ratio between the number of epoch elements of the observed value and the number of epoch elements of the cycle jump. The smaller the ratio is, the more serious the cycle jump is and the worse the quality of data collection is.

It is generally considered that the original data of the receivers with data integrity rate greater than 90%, MP1 and MP2 less than 0.5m, and cycle slip ratio greater than 4000 are qualified.

5) CODE MINUS CARRIER

Code minus carrier (CMC) is the difference between the observed value of pseudorange and the observed value of carrier phase. The size reflects the noise level of the pseudorange observations is reflected by the size. The formula can be expressed as:

$$CMC = P - L \tag{14}$$

III. NHC + ZUPT BDS PPP / INS TIGHT COUPLING

BDS PPP/INS tight coupled navigation can provide users with high-precision position, velocity and attitude information services. However, in the complex environment where the satellite is completely blocked and the structure of the visible satellite is not well distributed, there are discontinuities in the positioning results. How to deal with these errors is particularly important. Using external instruments or reference information can effectively reduce the positioning error of the integrated system, mainly including odometer, map matching, lidar, geomagnetism, slam and other auxiliary satellite/inertial integrated navigation. Without adding external instruments, the enhanced satellite/inertial integrated navigation system can be built according to the specific environment, mainly including velocity NHC, robust adaptive model and ZUPT. This section focuses on the methods of suppressing error accumulation in the absence of satellite signals.

A. NHC BDS PPP / INS TIGHT COUPLING

The navigation system only relies on the solution of inertial navigation when the vehicle is running in the environment where the satellite such as tunnel and underground garage is completely unlocked. Without other external constraints, the navigation error will increase rapidly. According to the particularity of land vehicle driving: assuming that the vehicle does not jump or slip during driving, the NHC calculation is used to suppress the rapid accumulation of errors. NHC principle was shown in Figure 1:

The constraint velocity perpendicular to the vehicle's forward direction is zero:

$$V^b = \begin{bmatrix} v_x^b \\ v_y^b \\ v_z^b \end{bmatrix} = \begin{bmatrix} v_x^b \\ 0 \\ 0 \end{bmatrix} \tag{15}$$

where v_x^b, v_y^b and v_z^b respectively represent the velocity in the front, right and up directions in the carrier coordinate system (as shown in Figure 1). The relationship between the calculated velocity in the carrier coordinate system and the velocity in the navigation coordinate system is as follows:

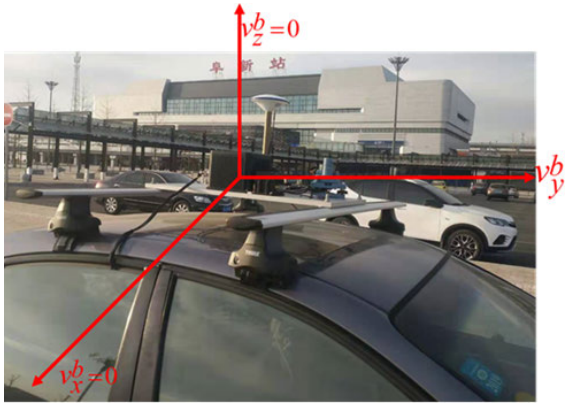

FIGURE 1. NHC principle.

$$V^b = \left(C_n^b\right)^T V^n \tag{16}$$

The error perturbation equation of the above formula is:

$$V^b + \delta V^b = \left(\left(I - \delta\varphi\times\right) C_n^b\right)^T \left(V^n + \delta V^n\right) \tag{17}$$

By expanding the above formula and keeping it to the first-order term, then:

$$V^b - C_n^b V^n + \delta V^b = C_n^b \delta V^n - C_n^b \left(V^n\times\right) \delta\varphi \tag{18}$$

where $\delta\varphi$ represents the attitude angle error. For the convenience of formula writing, define:

$$C_n^b = \begin{bmatrix} C_{11} & C_{12} & C_{13} \\ C_{21} & C_{22} & C_{23} \\ C_{31} & C_{32} & C_{33} \end{bmatrix} \tag{19}$$

Equation (15), equation (18) and equation (19) are combined, and the observation equation of NHC can be obtained as follows:

$$Z_{NHC} = \begin{bmatrix} 0 - \left(C_{21}V_E + C_{22}V_N + C_{23}V_U\right) \\ 0 - \left(C_{31}V_E + C_{32}V_N + C_{33}V_U\right) \end{bmatrix} \tag{20}$$

where V_E, V_N and V_U represents the velocity in the E, N, and U directions.

The differential form of equation (16) is expressed as:

$$\delta V^b = C_n^b \delta V^n - C_n^b \left(V^n\times\right) \delta\varphi \tag{21}$$

where $V^n\times$ represents the antisymmetric matrix composed of the velocity vector:

$$\left(V^n\times\right) = \begin{bmatrix} 0 & -V_U & V_N \\ V_U & 0 & -V_E \\ V_N & V_E & 0 \end{bmatrix} \tag{22}$$

According to the above formulas, the measurement matrix corresponding to the NHC observation equation (only the

terms related to position, velocity and attitude are given) is as follows:

$$H_{NHC} = \begin{bmatrix} 0_{1*3} & C_{2,1\sim3} & C_{2,1\sim3}(V^n\times) \\ 0_{1*3} & C_{3,1\sim3} & C_{3,1\sim3}(V^n\times) \end{bmatrix} \quad (23)$$

where $C_{i,1\sim3}$ represents the corresponding elements of columns 1 to 3 of the ith row (i = 2, 3) in C_n^b.

NHC BDS PPP/INS tightly coupled schematic diagram was shown in Figure 2. It should be noted that the premise of using velocity NHC is that the condition of no sideslip and no jump occurs during the driving process of land vehicles, while the actual carrier operation process does not necessarily meet this condition. So only when the satellite observation information is completely missing can this method be used to restrain the accumulation of positioning errors. PPP/INS tight coupling model is used when BDS observation information is available.

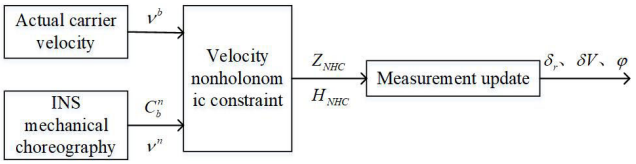

FIGURE 2. NHC BDS PPP/INS tightly coupled schematic diagram.

B. ZUPT BDS PPP/INS TIGHT COUPLING

When the carrier is static for a period of time (such as waiting for the traffic light), ZUPT is used to improve the accuracy of integrated navigation. When the carrier is static, then:

$$V^b = \begin{bmatrix} 0 & 0 & 0 \end{bmatrix}^T \quad (24)$$

Combined with the formula of BDS PPP/INS tight coupling, the observation vector of ZUPT BDS PPP/INS tight coupling is:

$$Z_{ZUPT} = \begin{bmatrix} 0-(C_{11}V_E + C_{12}V_N + C_{13}V_U) \\ 0-(C_{21}V_E + C_{22}V_N + C_{23}V_U) \\ 0-(C_{31}V_E + C_{32}V_N + C_{33}V_U) \end{bmatrix} \quad (25)$$

The corresponding measurement matrix is:

$$H_{ZUPT} = \begin{bmatrix} 0_{3*3} & C_n^b & C_n^b(V^n\times) \end{bmatrix} \quad (26)$$

The essence of the zero-velocity update is the same as the fine alignment principle of INS, but the difference is that the zero-velocity update requires judging whether the carrier is in a static state according to the BDS PPP/INS integrated navigation results. Assuming that the vehicle does not flameout in a static state, considering the influence of engine jitter and the velocity measurement error of BDS PPP/INS tight coupling based on extended Doppler, the threshold value selected in this paper is $w_0 = 0.5$ m/s, that is, when the horizontal velocity is continuously less than 0.5 m/s, it is considered to be a static state, and the zero-velocity update is adopted to perform measurement update.

Based on the above analysis of NHC and ZUPT, the NHC+ZUPT BDS PPP/INS tight coupling method was used to improve the positioning accuracy. The algorithm flowchart was shown in Figure 3:

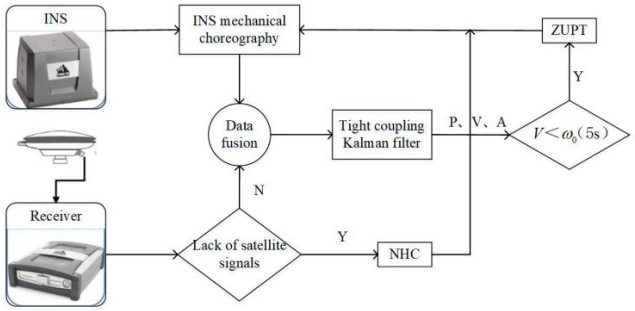

FIGURE 3. NHC+ZUPT BDS PPP/INS tightly coupled flowchart.

IV. EXPERIMENTAL RESULTS AND ANALYSIS

In this section, the experiment and result analysis of the above methods were carried out. In the BDS PPP positioning experiment, static data experiments and dynamic positioning experiments showed that the BDS PPP positioning accuracy after convergence was good. The NHC+ZUPT BDS PPP/INS tight coupled continuous positioning method was proposed, which the velocity NHC was used to limit the accumulation of errors, and the ZUPT correction principle was used to increase the navigation accuracy of the integrated system when the vehicle was stationary at the traffic lights. The results showed that the method could effectively restrain the accumulation of positioning errors of the navigation system in complex environment.

A. EXPERIMENT OF BDS DATA QUALITY ANALYSIS

The data quality is analyzed according to the main test indexes. The data integrity rate, MP1, MP2 and cycle to trip ratio analysis results of the total 24-hour original observation data from March 27 to 28, 2019 of measurement receiver produced by Zhong Haida was shown in Table 1. The values of MP1 and MP2 were calculated according to the Equation (11) and Equation (12) respectively. It could be seen from Table 1 that the data quality of the four satellite systems obtained by the receiver has reached the reference value, and the data quality of BDS was slightly better than that of GPS.

TABLE 1. Analysis of data quality of Hi-target measurement receiver.

	Data integrity rate/%	MP1(m)	MP2(m)	Cycle slip ratio
GPS	97	0.09	0.18	78676
BDS	97	0.08	0.09	979822
GLONASS	98	0.06	0.08	46066
GALILEO	94	0.19	0.13	9279

The pseudorange observation noise of BeiDou satellite and GPS satellite is compared with the original observation data of Trimble ALLOY receiver UTC time on March 1, 2019.

As shown in Figure 1, the pseudorange observation noise of BeiDou satellite's B1I frequency point and GPS L1 frequency point.

As shown in Figure 4, the accuracy of frequency pseudorange observation of B1I of the three BeiDou satellites was below 4 m, which was better than that of the two BeiDou satellites on the whole. The accuracy of the pseudorange observations of BeiDou satellite B1I and GPS L1 was the same, both of them were within 6 m, only GPS 09 satellite was slightly less accurate, and the noise of the pseudorange observations was about 6.2 m.

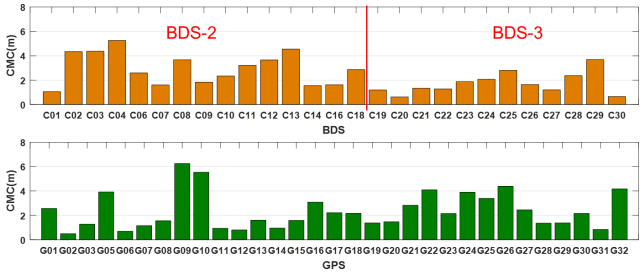

FIGURE 4. CMC of BDS and GPS satellite.

B. POSITIONING EXPERIMENT AND ACCURACY ANALYSIS OF BDS PPP

The accuracy and convergence time of BDS PPP were analyzed by static data experiment and vehicle dynamic experiment. Since the BDS-3 system officially started to provide services on December 27, 2018, the IGS analysis center of Wuhan University began to release BDS-3 precise ephemeris and clock difference products for a period of time. All the data in this paper before December 27, 2018 were solved by using BDS B1I frequency points and B2I frequency points, and the data after this time were solved by using BDS B1I frequency points and B3I frequency points.

1) STATIC EXPERIMENT

The static experimental data was the 24-hour simultaneous observation data of 4 Trimble ALLOY receivers provided by the National Basic Geographic Information Center. The data collection time was March 01, 2019, and the sampling interval of the receiver was 30s. The distribution of each measurement site was shown in Figure 5:

As shown in Figure 5, the farthest distance between the four stations was 116 km, and the shortest distance was 41 km [30]. The precision track and clock difference products provided by the IGS Analysis Center of Wuhan University were used for calculation, and the results of post-processing combined network adjustment calculation were used as reference values. The BDS PPP positioning error sequence of HRB2, HRYQ, HRSC and SHSZ stations were shown in Figure 6. The convergence time of BDS PPP was determined according to the standard that the three-dimensional error of ten consecutive epoch was less than 10cm, and the root mean square (RMS) was all the epoch after convergence. The

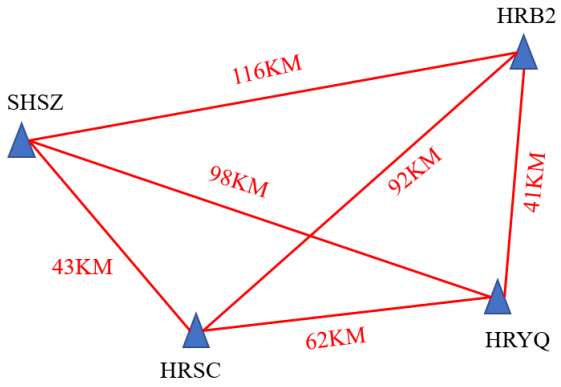

FIGURE 5. Distribution of four stations.

results of the root mean square errors and convergence time of four stations were shown in Table 2.

TABLE 2. HRB2, HRYQ, HRSC and SHSZ stations positioning RMS and convergence time.

Instrument station	*E* (cm)	*N* (cm)	*U* (cm)	Convergence time (min)
HRB2	0.9	1.1	1.3	58
HRYQ	0.8	1.0	1.1	28
HRSC	0.6	0.7	0.8	36
SHSZ	0.7	0.9	1.2	40

According to the results in Table 2, the horizontal positioning accuracy of BDS PPP after convergence was about 1 cm, and the accuracy in up direction was also within 1.5 cm, indicating that BDS PPP could fully meet the needs of high-precision positioning users. The average convergence time of the four stations was 40.5min, the longest convergence time was 58min for HRB2, and 28min for the shortest HRYQ. The three-dimensional accuracy was better than 10cm.

2) VEHICLE DYNAMIC EXPERIMENT

The vehicle experimental data was collected on April 27, 2019. and the data duration was 1h25min. The specific parameters were shown in Table 3. The starting point was Fuxin Railway Station, and the end point was School of Geomatics, Liaoning Technical University. The whole data acquisition time was about 940s, and the sampling interval was 1s. Pos-520 integrated navigation equipment was used as the experimental equipment. At the same time, it was assumed that there was a reference station on the roof of School of Geomatics. The positioning result calculated by RTK/INS was used as the positioning reference of vehicle experiment.

The comparison of BDS PPP and RTK/INS integrated navigation trajectory was shown in Figure 7, in which the red marker points were the positions of the integrated navigation calculation and the green marker points were the positioning results of BDS PPP. As shown in Figure 7 that the two positioning points basically coincided on the open road with good observation environment (red box in the figure).

TABLE 3. Vehicle experimental description.

UTC	Place	Sampling rate	Receiver	INS	Velocity	Reference
2019-4-27 5:12-6:37	Fuxin city	1 Hz	NovAtel	MP-POS520	~10 m/s	BDS/GPS RTK /INS

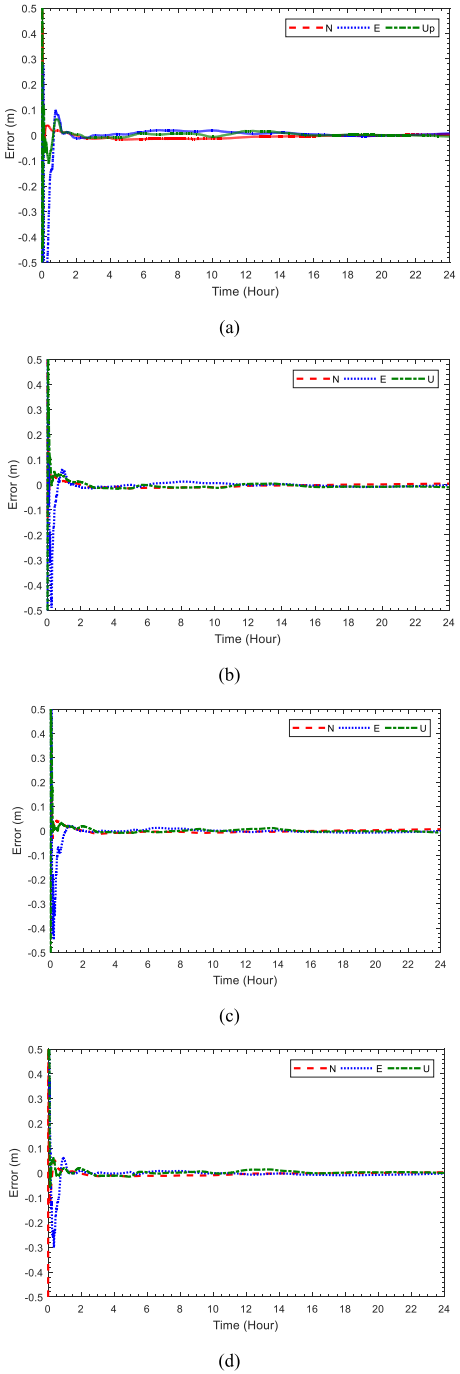

FIGURE 6. BDS PPP error of HRB2, HRYQ, HRSC and SHSZ. (a) HRB2; (b) HRYQ; (c) HRSC; (d) SHSZ.

The Yellow ellipse mark in the figure was the road near the building of School of Geomatics. Because the receiver signal was blocked by the building, the BDS PPP positioning results were quite different from the integrated positioning results, and even the positioning results could not be output.

FIGURE 7. Trajectory comparison between BDS PPP and RTK/INS integrated navigation.

The position error sequence of BDS PPP was shown in Figure 8. Due to the short acquisition time of vehicle dynamic experiment, the position of BDS PPP was not converged, and the receiver signal is blocked by the building when driving to the road near the building, so the position error was large. According to the statistics, the position accuracy of all three directions of the epochs was 0.80m, 0.59m and 2.08m respectively. The convergence time of PPP was still an important factor restricting its application in the field of high-precision navigation.

C. TIGHT COUPLED VEHICLE DYNAMIC POSITIONING EXPERIMENT OF BDS PPP / INS

Due to the large positioning error of BDS PPP in dynamic experiment, the NHC+ZUPT BDS PPP/INS tight coupling

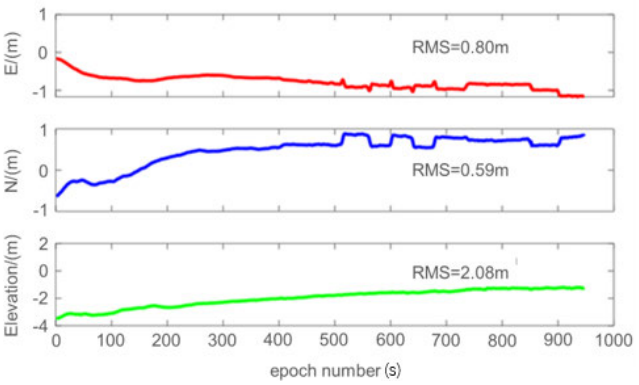

FIGURE 8. BDS PPP positioning error of vehicle experiment.

algorithm was proposed to improve the positioning accuracy in vehicle dynamic experiment. MP-POS520 integrated navigation equipment was used in the experiment, and the results of the post-processing calculation through the GINS software were taken as the reference values. The accuracy and IMU parameters were shown in Table 2.

The vehicle experiment track was shown in Figure 9. As shown in Figure 9, the whole vehicle experiment was carried out in Fuxin urban area, passing through the complex environment such as the road area under the viaduct and near the high-rise building (urban canyon). The vehicle was static for 15 minutes before it started, and initial alignment was performed at this stage to provide an initial attitude matrix for integrated navigation. BDS satellite number and position dilution of precision (PDOP) values for the entire vehicle experiment were shown in Figure 10. As it shown that the BDS satellite signal was unlocked frequently, and was missing during the experiment. The various driving environments in practical applications were fully reflected by the set of experimental data.

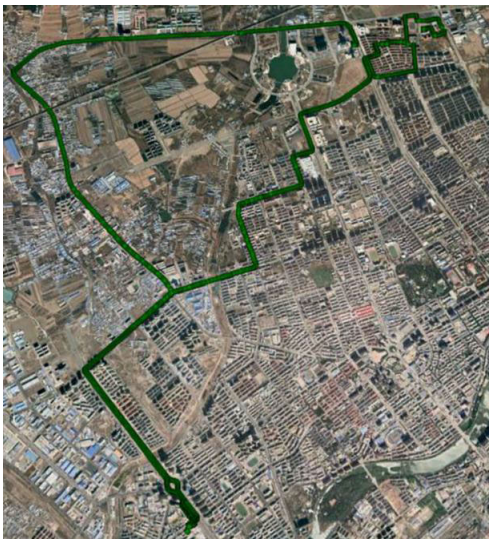

FIGURE 9. Vehicle experiment's trajectory.

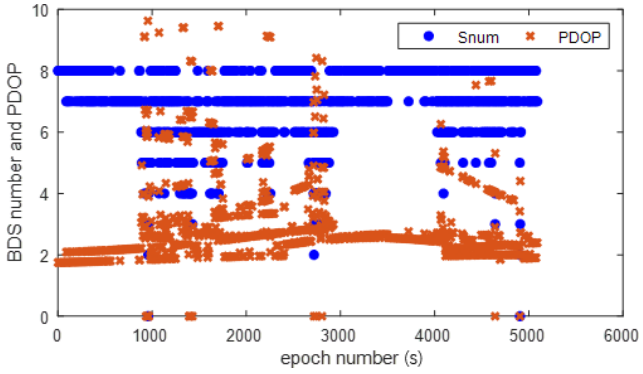

FIGURE 10. BDS satellite number and PDOP.

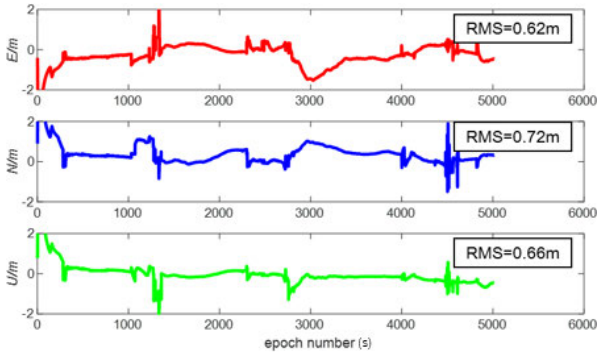

FIGURE 11. Vehicle experiment BDS PPP/INS tightly coupled positioning error.

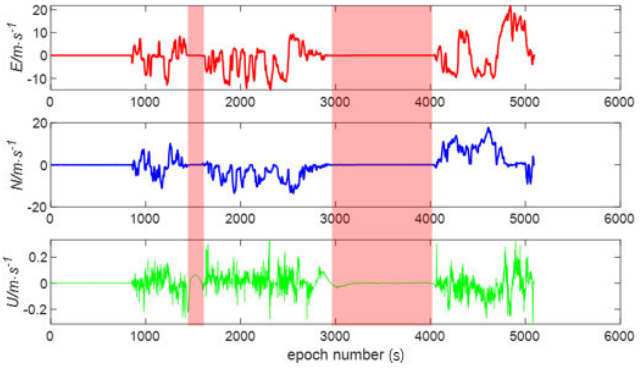

FIGURE 12. Vehicle experiment's velocity.

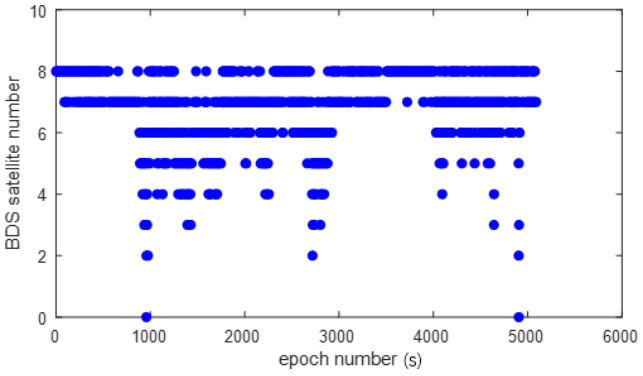

FIGURE 13. BDS satellite number.

The position error sequences of BDS PPP/INS tight coupling was shown in Figure 11. Due to frequent satellite interruption and satellite lock out in the experiment, the positioning accuracy was decimeter level, and the RMS in E, N and U directions were 0.62m, 0.72m and 0.66m, respectively. Compared in Figure 10 that the period with large position error mainly occured when the number of observation satellites was small and the PDOP values were large, mainly because the satellite ambiguity parameter needed to be recalculated after the satellite losed lock, and there was a certain convergence time. During the period when the observation

TABLE 4. MP-POS 520 precision and IMU parameters.

System performance	Positioning accuracy	Horizontal	0.02m	Up	0.03m
	Velocity accuracy	Horizontal	0.02m/s	-	-
	Attitude accuracy	Heading	0.08°	Attitude	0.05°
IMU parameters	Gyroscope (optical fiber)	Zero bias	0.1°/h	Zero bias stability	0.1°/h
	Accelerometer	Zero bias	25mGal	Zero bias stability	25mGal

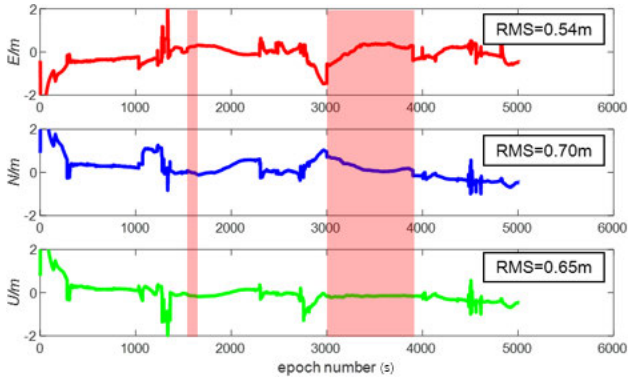

FIGURE 14. NHC+ZUPT BDS PPP/INS tightly coupled positioning error.

environment was good, the accuracy of BDS PPP/INS tight coupling could reach centimeter level.

NHC+ZUPT BDS PPP/INS tight coupling was used for calculation. The reference velocity of the vehicle experiment was shown in Figure 12, and the first 15min of the vehicle experiment was also in a static state, the process was the initial alignment, and the essence was also ZUPT. The red shaded part in the figure was the static state of the vehicle, and the ZUPT was used to constrain the tight coupling of BDS PPP/INS. For the convenience of description, the observation data of BeiDou satellite was shown in Figure 13. When the satellite was completely unlocked, the velocity NHC was enabled.

It could be seen from the red shaded part in Figure 14 that the accuracy of BDS PPP/INS integrated positioning under ZUPT constraint was high when the vehicle was static. As a whole, compared with PPP/INS tight coupled positioning results (as shown in Figure 11) without any constraints (RMS of E, N and U directions were 0.62m, 0.72m and 0.66m respectively), the accuracy of this method in E, N and U directions were improved by 8cm, 2cm and 1cm respectively.

V. CONCLUSION

Firstly, the observation equation, parameter estimation, fuzziness, degree of freedom, noise and other aspects of the ionospheric composite model were analyzed in depth. The BDS PPP dynamic positioning model based on the software to realize the ionospheric composite was established, and the errors that affect the positioning accuracy and convergence rate were analyzed and processed. The results of static data showed that the horizontal positioning accuracy of converged BDS PPP was better than 5cm, the vertical positioning accuracy was better than 10cm, and the difference between the dynamic positioning results and the high-precision RTK/INS integrated navigation results was less than 1cm. The BDS PPP/INS tight coupled continuous positioning of NHC+ZUPT was put forward. According to the problem of increasing positioning error with the increase of navigation time when satellite signals such as viaducts and tunnels were completely lack, combining with the characteristics of land vehicles, the accumulation of velocity NHC was used to limit the error, and the ZUPT was used to increase the navigation accuracy of the integrated system when the vehicle was driving in the static state at the traffic light. The experimental results showed that the accumulation of positioning errors could be effectively suppressed by this method in complex environment.

ACKNOWLEDGMENT

The authors would like to thank the technical support by Dr.Shunli Duan and thank the National Geomatics Center of China for providing GNSS data.

REFERENCES

[1] J. F. Zumberge, M. B. Heflin, D. C. Jefferson, M. M. Watkins, and F. H. Webb, "Precise point positioning for the efficient and robust analysis of GPS data from large networks," *J. Geophys. Res., Solid Earth*, vol. 102, no. 3, pp. 5005–5017, Mar. 1997.

[2] J. Kouba and P. Héroux, "Precise point positioning using IGS orbit and clock products," *GPS Solutions*, vol. 5, no. 2, pp. 12–28, Oct. 2001.

[3] Y. Gao and X. Shen, "A new method for carrier-phase-based precise point positioning," *Navigation*, vol. 49, no. 2, pp. 109–116, Jun. 2002.

[4] M. Ge, G. Gendt, M. Rothacher, C. Shi, and J. Liu, "Resolution of GPS carrier-phase ambiguities in precise point positioning (PPP) with daily observations," *J. Geodesy*, vol. 82, no. 7, pp. 389–399, Jul. 2008.

[5] F. N. Teferle, E. J. Orliac, and R. M. Bingley, "An assessment of Bernese GPS software precise point positioning using IGS final products for global site velocities," *GPS Solutions*, vol. 11, no. 3, pp. 205–213, May 2007.

[6] B. Zhang, J. Ou, Y. Yuan, and S. Zhong, "Precise point positioning algorithm based on original dual-frequency GPS code and carrier-phase observations and its application," *Acta Geodaetica et Cartographica Sinica*, vol. 39, no. 5, pp. 478–483, 2010.

[7] H. Zhang, Z. Gao, X. Niu, and Y. Wu, "Research on GPS precise point positioning with un-differential and un-combined observations," *Geomatics Inf. Sci. Wuhan Univ.*, vol. 38, no. 12, pp. 1396–1399, 2013.

[8] B. Li, H. Ge, and Y. Shen, "Comparison of ionosphere-free, UofC and uncombined PPP observation models," *Acta Geodaetica Cartograph. Sinica*, vol. 44, no. 7, pp. 734–740, 2015.

[9] J. Shi and Y. Gao, "A comparison of three PPP integer ambiguity resolution methods," *GPS Solutions*, vol. 18, no. 4, pp. 519–528, Oct. 2014.
[10] Y. Ge, P. Dai, W. Qin, X. Yang, F. Zhou, S. Wang, and X. Zhao, "Performance of multi-GNSS precise point positioning time and frequency transfer with clock modeling," *Remote Sens.*, vol. 11, no. 3, p. 347, Feb. 2019.
[11] J. Chen, J. Wang, Y. Zhang, S. Yang, Q. Chen, and X. Gong, "Modeling and assessment of GPS/BDS combined precise point positioning," *Sensors*, vol. 16, no. 7, p. 1151, Jul. 2016.
[12] J. Aggrey and S. Bisnath, "Improving GNSS PPP convergence: The case of atmospheric-constrained, multi-GNSS PPP-AR," *Sensors*, vol. 19, no. 3, p. 587, Jan. 2019.
[13] S. Ye, "Theory and realization of GPS precise point positioning using undifferenced phase observation," Ph.D. dissertation, Dept. Geodesy Geomatics, Wuhan Univ., Wuhan, China, 2002.
[14] J. Liu and S. Ye, "GPS precise point positioning by using undifferenced phase observation," *Geomatics Inf. Sci. Wuhan Univ.*, vol. 27, no. 3, pp. 234–240, 2002.
[15] T. Geng, Q. Zhao, J. Liu, and R. Du, "Real-time precise point positioning based on PANDA software," *Geomatics Inf. Sci. Wuhan Univ.*, vol. 32, no. 4, pp. 343–350, 2007.
[16] R. Ma and C. Shi, "Precise point positioning research based on BeiDou navigation satellite system," *J. Navigat. Positioning*, vol. 1, no. 2, pp. 7–10, 2013.
[17] X. Zhang, X. He, and X. Li, "Analysis of undifferenced kinematic POD for LEOs using TriP," *Geomatics Inf. Sci. Wuhan Univ.*, vol. 35, no. 11, pp. 1327–1330, 2010.
[18] B. Bahadur and M. Nohutcu, "PPPH: A MATLAB-based software for multi-GNSS precise point positioning analysis," *GPS Solutions*, vol. 22, no. 4, p. 113, Oct. 2018.
[19] N. Kjørsvik, J. Gjevestad, and E. Brøste, "Tightly coupled precise point positioning and inertial navigation systems," in *Proc. Int. Calibration Orientation Workshop (EuroCOW)*, 2010, pp. 1–6.
[20] S. Du and Y. Gao, "Inertial aided cycle slip detection and identification for integrated PPP GPS and INS," *Sensors*, vol. 12, no. 11, pp. 14344–14362, Oct. 2012.
[21] Y. Liu, F. Liu, Y. Gao, and L. Zhao, "Implementation and analysis of tightly coupled global navigation satellite system precise point positioning/inertial navigation system (GNSS PPP/INS) with insufficient satellites for land vehicle navigation," *Sensors*, vol. 18, no. 12, p. 4305, Dec. 2018.
[22] F. Wu, "Error compensation and extension of adaptive filtering theory in GNSS/INS integrated navigation," Ph.D. dissertation, Dept. Surveying Mapping, Inf. Eng. Univ., Zhengzhou, China, 2010.
[23] F. Zhu, "Key technology and algorithm realization of PPP/SINS integrated navigation," M.S. thesis, Dept. Geodesy Geomatics, Wuhan Univ., Wuhan, China, 2015.
[24] S. Liu, F. Sun, L. Zhang, W. Li, and X. Zhu, "Tight integration of ambiguity-fixed PPP and INS: Model description and initial results," *GPS Solutions*, vol. 20, no. 1, pp. 39–49, Jan. 2016.
[25] H. Han, J. Wang, and Z. Li, "Inertial aided kinematic GPS cycle slip detection and correction for GPS/INS tightly coupled system," *Acta Geodaetica et Cartographica Sinica.*, vol. 44, no. 8, pp. 848–857, 2015.
[26] Z. Li, "Precise point positioning and inertial measurement integrated navigation system enhanced with multi-sensor," Ph.D. dissertation, Dept. Environ. Spatial Inform., China Univ. Mining Technol., Xuzhou, China, 2015.
[27] Z. Gao, "Research on the methodology and application of the integration between the multi-constellation GNSS PPP and inertial navigation system," Ph.D. dissertation, Dept. Geodesy Geomatics, Wuhan Univ., Wuhan, China, 2016.
[28] Z. Gao, M. Ge, W. Shen, Y. Li, Q. Chen, H. Zhang, and X. Niu, "Evaluation on the impact of IMU grades on BDS + GPS PPP/INS tightly coupled integration," *Adv. Space Res.*, vol. 60, no. 6, pp. 1283–1299, Sep. 2017.
[29] J. Shi, G. Wang, X. Han, and J. Guo, "Impacts of satellite orbit and clock on real-time GPS point and relative positioning," *Sensors*, vol. 17, no. 6, p. 1363, Jun. 2017.
[30] J. Shi, C. Ouyang, Y. Huang, and W. Peng, "Assessment of BDS-3 global positioning service: Ephemeris, SPP, PPP, RTK, and new signal," *GPS Solutions*, vol. 24, no. 3, 2020.

WEI SUN was born in 1984. He is currently a Professor with the College of Geomatics, Liaoning Technical University, and also a Tutor of Ph.D. students. His research interest includes inertial and integrated navigation.

YIHAN YANG was born in 1994. She is currently pursuing the Ph.D. degree with Liaoning Technical University. Her research interest includes inertial and magnetic multi-source integrated navigation.